Ab initio study of ultrafast laser-induced spin flip, spin-flip transfer, and spin crossover in $Co_mBz_n^{+/0}$ clusters ($m, n = 1, 2$)

Na Zhang,[1] Hong Du,[1] Jun Chang,[1] Wei Jin,[1,2,*] Chun Li,[3] Georgios Lefkidis,[2] and Wolfgang Hübner[2]

[1]*School of Physics and Information Technology, Shaanxi Normal University, Xi'an 710119, China*

[2]*Department of Physics and Research Center OPTIMAS, Technische Universität Kaiserslautern, PO Box 3049, 67653 Kaiserslautern, Germany*

[3]*School of Mechanics, Civil Engineering and Architecture, Northwestern Polytechnical University, Xi'an 710072, China*

(Received 1 July 2018; published 27 September 2018)

We present a fully *ab initio* study of the laser-induced ultrafast magnetization dynamics in cobalt-benzene clusters $Co_mBz_n^{+/0}$ ($m, n = 1, 2$). It is found that different geometric configurations and d-π interactions of the four structures cause their high-level electronic structures to exhibit distinct characteristics. By using well-tailored laser pulses to propagate the systems via a spin-orbit-coupling enabled Λ process, various local/global spin-flip scenarios are achieved within subpicosecond timescales. Besides, a spin-flip-transfer process within around 300 fs is predicted in Co_2Bz. Governed by the Goodenough-Kanamori rules, the simultaneous spin flip and transfer is favored when the two magnetic centers are antiferromagnetically coupled, reflected in the required lowest laser energy and intensity. Most interestingly, we obtain a novel, W-process facilitated spin-crossover scenario in the cluster $CoBz^+$, which offers additional flexibility of designing relevant all spin-based functions such as molecular switches and sensors. The transferability of the latter two scenarios is also analyzed from the optical spectra of the initial and final states. These results provide the precursory guidance for further study of ultrafast magnetization control in more extended metal-aromatic polymers, and also show their great potential in future nanoscale spintronic applications and quantum information processing.

DOI: 10.1103/PhysRevB.98.104431

I. INTRODUCTION

With the increasing demand for large-density storage and high-speed processing in spintronics, optically induced ultrafast magnetization dynamics has become one of the most intriguing issues of magnetism in recent years [1–13]. Among a wide range of the involved magnetic materials ranging from bulk structures to alloy multilayers and even molecular magnets, nanoscale magnetic clusters/complexes attract more and more interest, due to their ultimately small size that enormously favors the enhancement of the information recording density and discrete energy levels that allow for manipulating magnetization states in a controllable way. Several stable spin-based nanologic elements, for instance, magnetic logic gates [14–17], spin shift register [18], and spin ERASE functionality [19] have been proposed. These can serve as the building blocks for constructing molecular spintronic devices and promote the development of future quantum computing or molecular computers [20].

Cobalt-benzene (Co-Bz) systems, being synthesizable by use of laser-evaporation techniques, are of great interest recently because of their unique physical and chemical properties. Numerous experimental [21–26] and theoretical [27–39] investigations concerning their fabrication, characterization, geometries, electronic structures, and magnetic properties have been reported. With respect to theoretical methods, density functional theory (DFT) approaches that highly depend on the exchange-correlation functionals are commonly employed. Besides, the quantum Monte Carlo method [36] and the complete active space self-consistent field (CASSCF) method [40] are also applied to investigate the structure, ionization/dissociation energy, and spin-dependent electronic gap of cationic cobalt-benzene systems and the adsorption of cobalt on a local structure of graphene, respectively. However, for the predictive study of ultrafast laser-induced spin dynamics in these systems, which requires a high-level, complete wave-function-based description, to the best of our knowledge, has not been reported yet.

In this paper we perform a fully *ab initio* quantum chemistry calculation on ultrafast spin dynamics in small (half-) sandwich Co-Bz clusters $Co_mBz_n^{+/0}$ ($m, n = 1, 2$). Different from the fullerene-encaged structures [41], where the magnetic centers are too isolated from the environment, and the ligand-stabilized structures [42,43], where the magnetic centers are too separated by the attachment of bridging atoms, these intermediate (half-)sandwich clusters are expected to exhibit new features for their spin dynamics. In addition, studying spin manipulation in these structures is fundamentally and technologically crucial for future spintronic applications, since it helps to understand the magnetic nature of larger systems such as complicated organometallic complexes, transition metal-benzene (TM-Bz) sandwich molecules bridging the tips of certain nanocontacts [33,38], and TM atoms adsorbed on monolayer or bilayer graphene [40,44–47]. All of them are promising to be realized in the present experiment and technology status. Most importantly, as basic building blocks, sandwich-type TM-Bzs are suggested to be possible

*jinwei@snnu.edu.cn

candidates for the functionality of spin filters/spin valves and information storage [31,48,49].

The paper is organized as follows. Section II introduces the computational method. Then, the structures, infrared spectra, and energy levels of the four systems are given in Sec. III. In Sec. IV the achieved ultrafast dynamics results of spin-flip (Sec. IV A), spin-flip-transfer (Sec. IV B), and spin-crossover (Sec. IV C) scenarios are presented and analyzed. Our summary follows in Sec. V.

II. THEORETICAL METHOD

In our *ab initio* study, the Hamiltonian of the strongly correlated systems is solved in three steps [43,50,51]. First, for the nonrelativistic part, by using the GAUSSIAN 16 package [52], the structural optimization and infrared spectra are performed at the Hartree-Fock (HF) level. The subsequent high-level electronic structures are calculated by applying the symmetry-adapted cluster configuration interaction (SACCI) method [53], which is capable of providing a more accurate description of the many-body problem by taking various virtual excitations and multiple effects of correlations into account. To keep the balance between accuracy and cost of calculating excited states of the strongly correlated systems, we choose the Lanl2dz basis set for Co and STO-3G for C and H atoms as a compromise. Before starting the dynamical part, in the second step we perturbatively introduce a static external magnetic field (with a strength of 10^{-5} atomic units) and spin-orbital coupling (SOC) to eliminate the degeneracy and obtain spin-mixed states that are required by the Λ process (i.e., a two-photon process comprising the absorption of an incident photon which excites the system from the initial state to the spin-mixed intermediate states, and the successive induced emission of a photon which de-excites from the intermediate states to the final state) [50,51]. Here effective nuclear charges are used to approximate the two-electron integrals [54,55] when calculating SOC. Then, a suitably tailored time-dependent laser vector potential is applied to stimulate the light-matter interaction. The time evolution of the system is described by a set of coupled differential equations [43,50,51] and solved with the fifth-order Runge-Kutta method with Cash-Karp adaptive step size [56]. Additionally, to efficiently achieve the desired dynamics with appreciable population transfer from the initial state to the final state, a genetic algorithm is adopted for optimizing the laser pulses [57].

III. STRUCTURES, INFRARED SPECTRA, AND ENERGY LEVELS

The four stable structures optimized at the HF level, together with their symmetries, spin multiplicities, and Co-C bond lengths, are shown in Fig. 1. The threshold values of the maximum component of the force and the root-mean square of the forces for the optimization step are less than 4.5×10^{-4} and 3.0×10^{-4} hartree/bohr, respectively. It turns out that the geometries of all of these structures take the form of half-sandwich or sandwich type, of which the stabilities are confirmed through the absence of imaginary frequencies of the normal modes. Especially for Co_2Bz_2, its sandwich geometry agrees with experimental suggestions [21–23] about

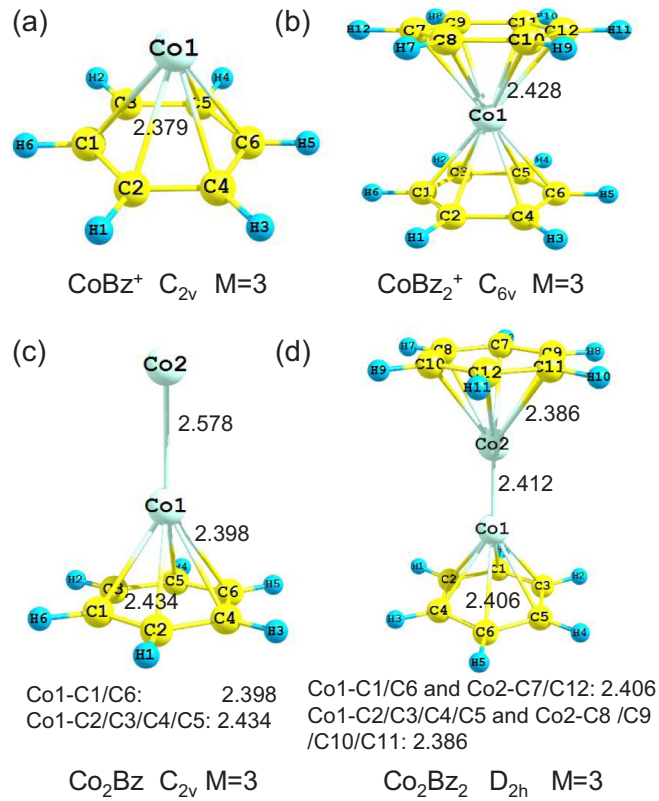

FIG. 1. The optimized geometries of $CoBz^+$, $CoBz_2^+$, Co_2Bz, Co_2Bz_2, and their symmetries as well as spin multiplicities. The Co-C bond lengths (in Å) are labeled.

the "riceball" arrangement in which central metal clusters are fully covered by Bz molecules (instead of the multidecker in which metal atoms and Bz are alternately piled up).

Here the cationic species for the mononuclear Co clusters ($CoBz^+$ and $CoBz_2^+$) are used, since the even number of electrons enables us to have a triplet system that allows for the separation of charge and spin dynamics. The lowest-energy configurations of them are both found to be triplet, which is consistent with Refs. [25,27,37]. However, some of the ground-state symmetries differ depending on the structural isomers considered and on the details of the computational methods applied. For example, C_{2v} [25] and C_{6v} [27,37] are almost degenerate in our calculation. The proposed triplet D_{6h} [25,27,37] configuration for $CoBz_2^+$ has lower energy than the obtained C_{6v} isomer. However, a vibration analysis yields imaginary frequencies, which means that this is not a stable geometry. This is also the case for predicting the spin multiplicities and geometries of the dinuclear Co clusters (Co_2Bz and Co_2Bz_2). In our study, the most reasonable and stable structure of Co_2Bz possesses C_{2v} symmetry and has spin multiplicity 3, while, with the same statement that the Co-Co bond is perpendicular to the centroid of the Bz ring, Ref. [35] indicates that its ground-state structure exhibits C_{2v} symmetry but in a quintet state (with energy 1.02 eV higher than the triplet C_{2v} configuration and one small imaginary frequency in our calculation), and Ref. [32] suggests a triplet C_{6v} configuration (which is not converged in our trials). For Co_2Bz_2, what we get is a triplet coaxial (here

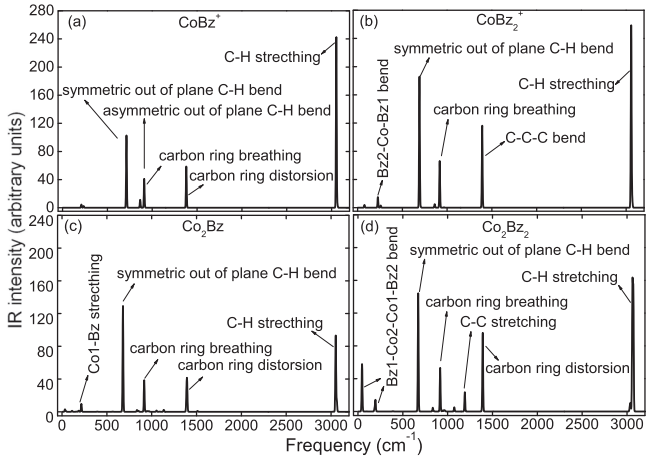

FIG. 2. IR spectra of the structures $CoBz^+$, $CoBz_2^+$, Co_2Bz, Co_2Bz_2 with the main vibrations with noticeable intensities characterized.

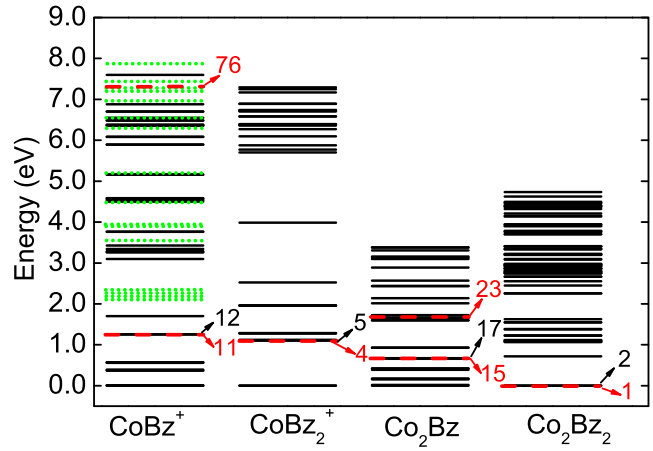

FIG. 3. Low-lying energy levels of the four structures after the inclusion of SOC and the external magnetic field. The initial and final states that involve in the spin dynamics to be discussed later are marked.

coaxial means the Co-Co bond is collinear with the C_2 axis of the whole structure) configuration exhibiting symmetry D_{2h}, while different spin states (singlet and triplet), symmetries (C_1 and D_{6h}), and conformations (coaxial and perpendicular) are suggested in different references [24,28,30,35]. Among these calculated isomers, the coaxial singlet D_{6h} [28] and singlet C_{2v} configurations are degenerate and lie 1.18 eV higher, the perpendicular triplet C_{2h} is 1.73 eV higher, while the perpendicular triplet C_1 [35] does not converge. As for the structural bondings and parameters, relative to $CoBz^+$, the Co-C distance of $CoBz_2^+$ increases from 2.379 to 2.428 Å due to an albeit small repulsion of the Bz units and the Co atom is now bonded with two ligands. For $Co_2Bz_{1,2}$, with the attachment of an additional Bz unit, the Co-Co bond length of Co_2Bz_2 turns to be shorter than that of Co_2Bz because the attachment of a Bz ring leads to a loss of $3d$ electrons per Bz attached [38] and thus reduces the repulsion of Co-Co.

Figure 2 shows the calculated vibrational spectra of the four structures at the HF level with the main normal modes characterized. Since Co is much heavier than C and H, except for the region of 0–250 cm^{-1} for Co-Bz vibrations, the IR spectra patterns of the Co-Bz clusters are almost the same as that of a Bz ring. Here a scaling factor of 0.823 for the basis STO-3G is applied for the comparison. Clearly the four spectra exhibit a similar feature with respect to the frequency values and relative infrared intensities of the main normal modes. Especially, the eigenvalues of the following three modes for benzene rings of these four structures, i.e., out of plane C-H bending, carbon-ring distortion (C-C-C bend for $CoBz_2^+$), and C-H stretching, are in the region of 679–713, 1380–1395, and 3050–3071 cm^{-1}, respectively. These values agree somehow with the experimental values [58,59] of 673, 1486, and 3047.3 cm^{-1}.

The low-lying ground and excited energy levels of the four structures after the inclusion of SOC (and the external magnetic field) are shown in Fig. 3, in which the initial and final states involving in the spin dynamics to be discussed later are marked. In each structure there are five lowest triplet terms before the inclusion of SOC for each irreducible representation being calculated, thus the number of triplet states of each cluster shown in Fig. 3 is 61 [i.e., $1 + 5 \times 4 \times 3$, here 1 refers to one reference SAC singlet state, 5 means five triplet terms, 4 denotes four irreducible representations for symmetry C_{2v}, and 3 is the number of states that each triplet term splits into after SOC), 61, 61, and 121, respectively. Five additional singlet terms for $CoBz^+$ are included for the purpose of illustrating the achieved spin-crossover dynamics later, contributing another 20 singlet states to its level scheme (green dotted lines in Fig. 3). The C_{6v} point group of the second structure is reduced to its largest Abelian subgroup C_{2v} in the SACCI calculation, thus four irreducible representations are considered. Higher multiplicities (quintets, septets, etc.) are not calculated since including them makes the computational cost much higher, while it does not bring any significant improvement in the spin dynamics, as we know from previous results.

Comparing the levels of the first and third structures and the levels of the second and fourth structures in Fig. 3, one can clearly notice that the level distribution of the Co_2-Bzs become denser in the low-energy range (e.g., below 2 eV) than that of the corresponding cationic Co-Bzs. This is due to the fact that an additional cobalt atom brings about more electrons and thus stronger $3d$ electron correlations which, in turn, produces more d-character states. On the other hand, comparing the triplet levels of the first and second structures and the levels of the third and fourth structures in Fig. 3, we find that the charge-transfer states (which are located at the high-energy region) of the Bz dimer clusters are more and denser than that of the corresponding mono Bz ones. We attribute it to the inductive-I effect of Bz since by attracting more electrons from Co the addition of a Bz ring can give rise to strong $3d$-π electron interactions and thus induce more charge-transfer (CT) states. Note that the inductive-I effect for the Bz ligands can be directly compared only for the two neutral clusters Co_2Bz (−0.566 on Bz, 0.237 on Co1 and 0.329 on Co2) and Co_2Bz_2 (−0.574 in each Bz and 0.574 on each Co). Clearly the charge density at the Co atoms increases

with the addition of the second Bz. In the case of the charged clusters $CoBz^+$ and $CoBz_2^+$ the redistribution of the charged density due to the removed electron renders the Bz ligands of the two clusters inequivalent, and thus their respective inductive-I effect not directly comparable.

According to these discussions, it is expected that, at least for the same type of spin dynamics (e.g., spin-flip scenarios), the laser energies for driving the spin dynamics in cationic Co-Bzs will be higher than that for the corresponding Co_2-Bzs, and the laser energies for driving the spin dynamics in Co-Bz half-sandwiches will be higher than that for corresponding sandwichlike structures. Both of them are caused by the possible involvement of higher-energy intermediate states during the dynamics propagation, but with different origins: substantial less d states for mono Co systems in the former case and more CT states for Bz dimer systems in the latter case.

Based on the high-level calculation of the ground and excited states of these many-body systems, after the inclusion of SOC and an external magnetic field, various ultrafast spin dynamics scenarios, including spin switching (with respect to the flip of spin direction), spin-flip transfer (with respect to the simultaneous change of spin localization and spin orientation), and spin crossover (with respect to the alteration of spin multiplicity) have been achieved driven by various suitably well-tailored time-resolved laser pulses. Note that the spin-flip and spin-transfer dynamics is governed by the time-dependent coupling of the spins as dictated by the Goodenough-Kanamori rules [60–62], which are commonly employed to describe the preferred static ferromagnetic/antiferromagnetic coupling of two nearby magnetic centers coupled by the superexchange interaction. The Goodenough-Kanamori rules are connected both to the global symmetry of the molecule and the local symmetry of the participating bonds. In the following we turn our attention to describe these scenarios and reveal their underlying physics, hoping to enrich our understanding of ultrafast magnetization control in Co-Bz clusters and stimulate future experimental efforts on their realization towards relevant spintronic applications.

IV. LASER-INDUCED ULTRAFAST SPIN DYNAMICS

A. Spin-flip scenarios

Figure 4 shows the spin-flip scenarios obtained in the four structures, all of which complete within subpicoseconds with high fidelity above 94%. The lower panel of each dynamics depicts the switching of a certain spin component (x-component spin for monobenzene clusters and z-component spin for dibenzene clusters) after the influence of the laser pulses. The detailed information of the initial and target states (stemming from the same triplet term before the inclusion of SOC) with opposite spin directions in each scenario, including their energies, spin expectation values and spin localizations is listed in Table I. It should be noted that normally the flip scenarios exhibit symmetric behavior (as shown in Fig. 4) because the two branches of the Λ process (initial-intermediate branch and intermediate-final branch) always have compara-

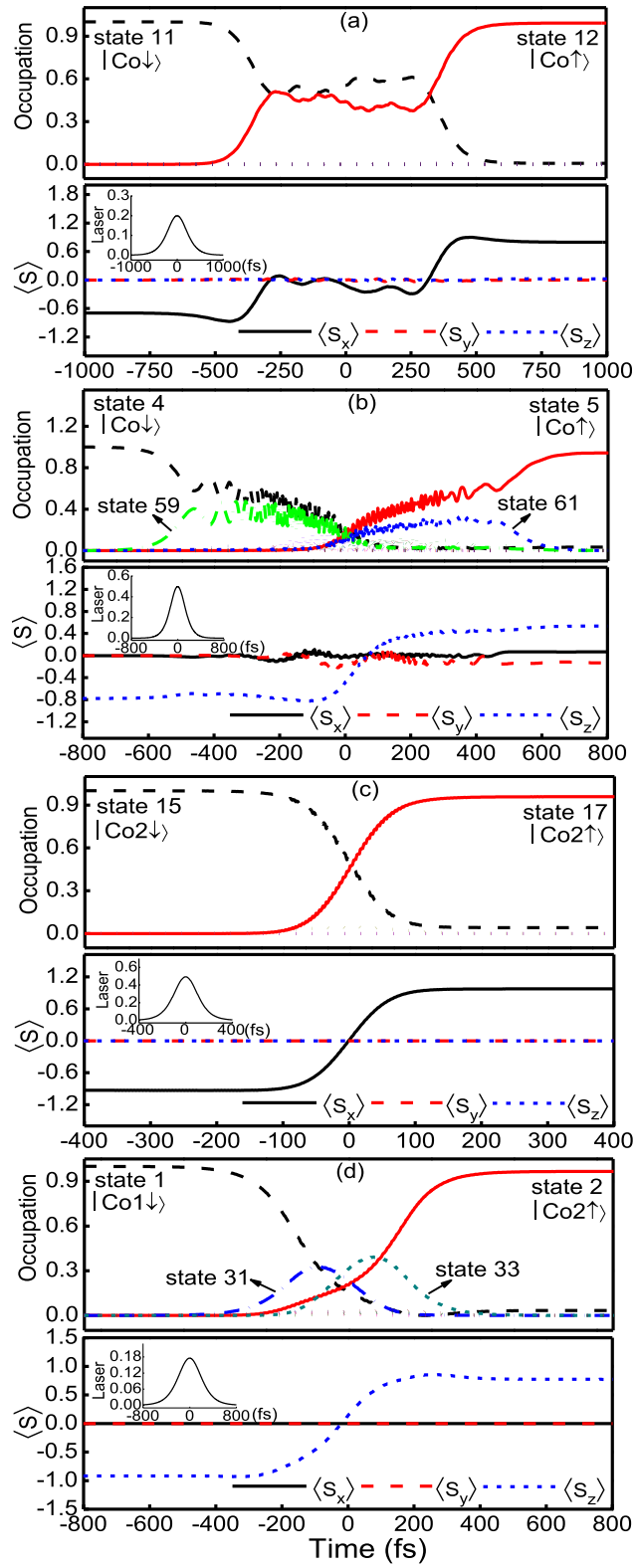

FIG. 4. Spin-flip processes in clusters $CoBz^+$ (a), $CoBz_2^+$ (b), Co_2Bz (c), and Co_2Bz_2 (d). For each scenario, the upper panel depicts the occupation probabilities of the involved states (initial: dashed, final: solid, intermediate: others), and the lower panel shows the time-dependent expectation values of the spin components. The intermediate states that show appreciable occupation during the propagation are marked, and the inset gives the envelope of the optimized laser pulse.

TABLE I. Energies, spin expectation values, and spin density of the initial and final states in the ultrafast spin-flip, spin-flip-transfer, and spin-crossover scenarios discussed in this paper.

Scenario	Structure	Initial and final states	Energy (eV)	$\langle S_x \rangle$	$\langle S_y \rangle$	$\langle S_z \rangle$	$\langle S \rangle$	Spin density Co1	Spin density Co2
Spin-flip	$CoBz^+$	initial: state 11	1.254	−0.678	0	0	0.678	−1.958	–
		final: state 12	1.256	0.678	0	0	0.678	1.958	–
	$CoBz_2^+$	initial: state 4	1.103	0	0	−0.784	0.784	−1.930	–
		final: state 5	1.105	0	0	0.784	0.784	1.930	–
	Co_2Bz	initial: state 15	0.664	−0.931	0	0	0.931	−0.029	−1.969
		final: state 17	0.665	0.931	0	0	0.931	0.029	1.969
	Co_2Bz_2	initial: state 1	0.000	0	0	−0.917	0.917	−0.972	−0.972
		final: state 2	0.001	0	0	0.917	0.917	0.972	0.972
Spin-flip-transfer	Co_2Bz	initial: state 17	0.665	0.931	0	0	0.931	0.029	1.969
		final: state 23	1.599	−0.845	0	0	0.845	−1.941	−0.007
Spin-crossover	$CoBz^+$	initial: state 12	1.256	0.678	0	0	0.678	1.958	–
		final: state 76	7.244	0	0	0	0	0	–

ble transition magnitudes due to the similar electronic properties of the initial and final states.

The related parameters of the driving laser pulses of the above spin-flip scenarios are listed in Table II. By comparing these parameters, we find that, at a cost of the relatively high laser intensity (6.39 J s^{-1} m^{-2}), the time of achieved spin switching process in Co_2Bz is the shortest (around 300 fs) and the corresponding required laser energy is the lowest (1.62 eV) among the four flip scenarios, which can be attributed to the involvement of only four intermediate states with energies (0.386, 0.417, 0.674, and 2.138 eV, respectively) nearby the initial and final states. Specifically, less intermediate states normally simplifies the dynamics and gives rises to a clear-cut dynamic behavior and the lower energy of intermediate states ensures a small laser detuning and thus a small laser energy. This is also consistent with the aforehand deduction about the lower laser energy required for driving spin dynamics in systems with more Co atoms and less Bz molecules. As for $CoBz^+$, among 19 (ten singlets and nine triplets) involved intermediate states, states 35 and 36 with energies 4.4980 and 4.4983 eV contribute to the dynamics appreciably with respect to their strong transition peaks [as can be seen in the latter discussion of absorption spectra of state 12 in Fig. 7(b)], and thus give a higher laser energy 2.98 eV (compared to that for Co_2Bz). Here the inclusion of singlets is because we find a spin-crossover scenario in the extended singlet-triplet subspace and thus perform again the switching dynamics using the same initial and final states as we obtained in the triplet subspace to avoid two sets of state notations. Actually, the involvement of singlets only slightly affects the dynamic behavior and the laser parameters (intensity, FWHM and energy), details can be found in the Appendix.

For cluster $CoBz_2^+$ with less Co atoms and more Bz molecules, its spin switching process, exhibiting a complicated pattern, completes within 700 fs [as shown in Fig. 4(b)]. As speculated from the discussion of its level distribution previously, the highest laser energy should be required. This is confirmed by our results since out of the total 23 intermediate states there are 16 being located at a high-energy region of 5.8–7.29 eV, which naturally leads to the extraordinarily highest laser energy (6.2 eV) among the four flip scenarios. Different from the above three local flip scenarios, the flip dynamics in Co_2Bz_2, however, is a global one since its two cobalt centers are indistinguishable due to the high symmetry D_{2h}. In addition, the laser that drives a spin-flip scenario in the structure with nonlocalized spin normally is less intense compared to that for a structure with well-localized spin. This

TABLE II. The optimized parameters of the laser pulses for the achieved ultrafast spin scenarios. Here θ and ϕ denote the angles of the incidence in spherical coordinates, and γ is the angle between the polarization of the light and the optical plane. FWHM is the full width at half maximum of the laser pulse.

Scenario	Structure	$P_{\text{final state}}$	Laser parameters θ (deg)	ϕ (deg)	γ (deg)	Intensity (J s^{-1} m^{-2})	FWHM (fs)	Energy (eV)
Spin-flip	$CoBz^+$	99.2%	66.2	209.0	331.1	1.05	500	2.98
	$CoBz_2^+$	94.2%	93.3	78.8	131.6	6.53	300	6.2
	Co_2Bz	95.8%	339.9	315.0	316.7	6.39	239	1.61
	Co_2Bz_2	96.6%	285.4	46.8	354.4	0.81	465	2.6
Spin-flip-transfer	Co_2Bz	84.9%	70.0	229.4	118.2	0.17	119	0.91
Spin-crossover	$CoBz^+$	75.4%	113.0	320.9	89.4	6.57	258	2.96

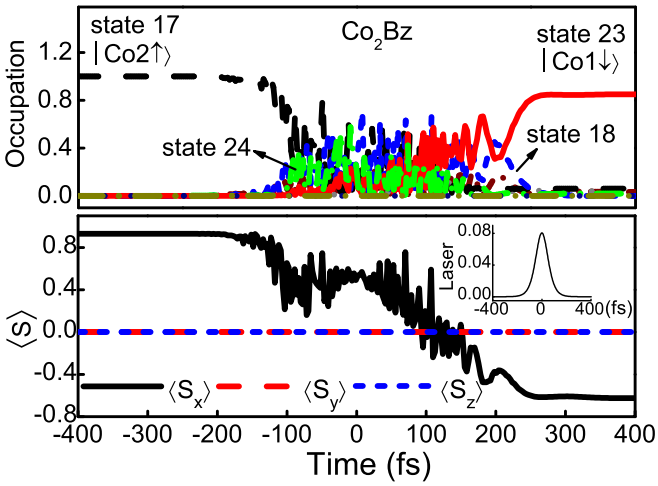

FIG. 5. Spin-flip-transfer scenario from Co2 to Co1 in the structure Co_2Bz. The upper panel depicts the occupation probabilities of the involved states (initial: dashed, final: solid, intermediate: dotted), and the lower panel shows the time-dependent expectation values of the spin components. The intermediate states which exhibit appreciable occupation during the propagation are indicated, and the inset shows the envelope of the optimized laser pulse.

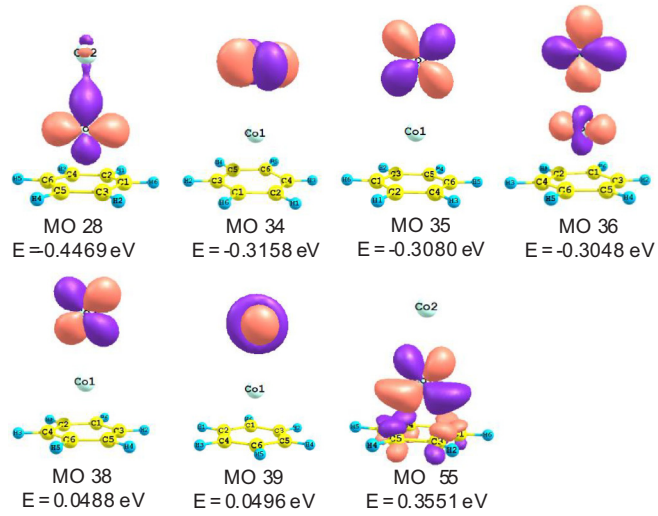

FIG. 6. The main d-character molecular orbitals of the structure Co_2Bz that make appreciable contributions to the virtual excitations for the initial and final states. The violet (dark) and orange (light) isosurfaces of the wave functions represent positive and negative values, respectively.

can explain to some extent the lowest intensity of the fourth dynamics scenario (see Table II).

As stated above, since the initial and final states of the spin-flip dynamics are chosen as the ones splitting from the same triplet term, the similar selection rules of the two branches of the Λ process makes the dynamics relatively easy and efficient. About this, some conclusive remarks have been addressed in detail in our previous work [43,51,63]. However, to satisfy the demands for certain industrial spintronic applications, the function of spin-flip manipulation is usually not enough. Altering spin localizations from one magnetic center to another center or changing spin state from high spin to low spin (or vice versa), although challenging to achieve, is particularly and urgently crucial, since this capability could offer more flexibility of designing additional related all spin-based functions that serve as promising building elements in the construction of future integrated spin-logic devices and quantum computer.

B. Spin-flip-transfer scenario

By choosing initial and final states with different spin localizations and setting an appropriate range of the laser parameters, we obtain a spin-flip-transfer scenario, i.e., a simultaneous spin-flip and spin-transfer process, in Co_2Bz, as shown in Fig. 5. For the other three structures where spin transfer cannot be performed, $CoBz^+$ and $CoBz_2^+$ have only one magnetic center, and Co_2Bz_2, as mentioned in the above subsection, has a higher symmetry of D_{2h} and its two cobalt atoms cannot be distinguished. According to Fig. 5, after the influence of the laser pulses (the parameters of which are listed in Table II), the initially occupied spin-up state, i.e., state 17 with spin localization on Co2, is transferred to the final spin-down state, i.e., state 23, the spin of which is localized on Co1, with a final occupation of 85%. The detailed information of the initial and final state, including the energy, spin expectation values and spin localizations, is given in Table I.

Before discussing the dynamics in detail, first we illustrate the origin of different spin localizations of the initial and final states. Figure 6 shows the main d-character molecular orbitals (MOs) that make appreciable contributions to the virtual excitations of the two states together with their orbital energies, from which the distinct electron-cloud localizations of the two magnetic atoms can be obviously noticed. As the initial state in the spin-flip-transfer scenario, state 17 stems from the fifth triplet term. Detailed analysis tells us there are three dominant contributions to this state, which are a single excitation from MO 35 (d_{yz}) to MO 39 (d_{y^2}) with coefficient 0.877, and two double excitations, i.e., MO 38 (d_{xz}) → MO 39 (d_{y^2}) (α excitation), MO 34 (d_{xy}) → MO 39 (d_{y^2}) (β excitation) with coefficient −0.433 and MO 36 ($d_{x^2-z^2}$) → MO 39 (d_{y^2}) (α excitation), MO 35 (d_{yz}) → MO 39 (d_{y^2}) (β excitation) with coefficient −0.415. Since all these relevant MOs show an electron-cloud distribution (mainly) on Co2, one can roughly deduce that spin is localized on the same magnetic center. Indeed, after taking all the existing excitations into account in our calculation, the final spin density of the three units for this state is 0.029 on Co1, 1.969 on Co2, 0.002 on Bz. Similarly, state 23 comes from the eighth triplet term and the largest contribution to this state is a single excitation from MO 28 ($d_{y^2-z^2}$) to MO 55(d_{xy}) with coefficient −0.82, which both exhibit electron-cloud localization on Co1. Including all the existing excitations we achieve a spin-density distribution of −1.941 on Co1, −0.007 on Co2, and −0.051 on Bz.

As can be seen in Fig. 5, the whole process exhibits a noticeable oscillation behavior and completes within 300 fs. It should be emphasized that, among all the scenarios discussed in the paper, the laser intensity (0.17 J s^{-1} m^{-2}), FWHM (119 fs), and energy (0.91 eV) of this spin-flip-transfer dynamics are all the smallest (see Table II). We attribute the easier dynamic feature to the originally allowed direct

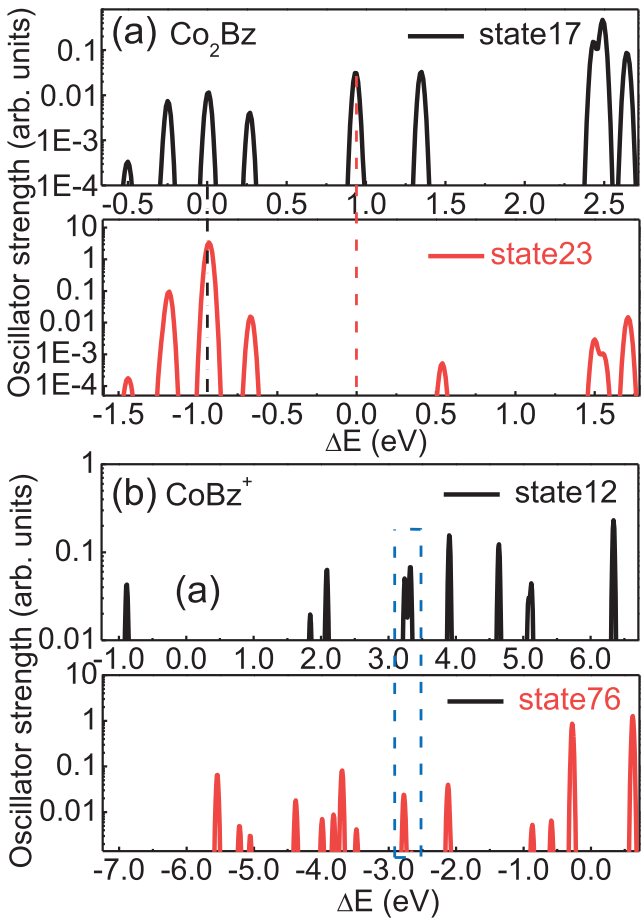

FIG. 7. Optical spectra of the initial and final states of (a) the spin-flip-transfer scenario in Fig. 5 and (b) the spin-crossover scenario in Fig. 8, respectively.

transition between the initial and final state and the small energy region ($E_{26} - E_{13} = 1$ eV) expanding by all the involved total six intermediate states (i.e., states 13, 15, 18, 24, 25, and 26 with energies 0.659, 0.664, 0.674, 1.6, 1.657, and 1.658 eV, respectively), to which the laser energy is almost resonant. As for the first factor, we calculate the absorption spectra of the initial and final states through the oscillator strength [42,43], as shown in Fig. 7(a). The abscissa denotes energy difference between the initial(/final) electronic state and other states, ranging from a minimum value of $-E_{\text{initial/final}}$ to a maximum value of $E_{\text{highest}} - E_{\text{initial/final}}$. In this way, the spectra of the two states can be compared directly since vertically the energy differences of the initial and the final states correspond to the same state. Clearly an allowed transition between them can be easily observed from the peaks at energy difference 0.934 eV (red dashed vertical line) for state 17 and −0.934 eV (black dash-dotted vertical line) for state 23, respectively, indicating their possible strong transferability. For such a direct transition, along with their several common peaks at lower energy region (e.g., below 1 eV), the search for higher-lying intermediate states can be automatically blocked by the selection routine during the system evolution and thus a less intense and lower-energy laser is adequate to fulfill the dynamics. Here a common peak in the two spectra shows the existence of an intermediate state coupling to both the initial and final states with the same resonance energy. Obviously, as dictated by the Goodenough-Kanamori rules, a simultaneous spin flip and transfer is much favored (cf. the laser parameters in Table II) if the two magnetic centers are antiferromagnetically coupled.

C. Spin-crossover scenario

Spin crossover, known as spin state transition between high spin (HS) and low spin (LS), has been investigated extensively due to its potential applications in various fields, such as molecular electronics, data storage, and display/switch devices [64,65]. It usually occurs in the transition metal-based molecular complexes exhibiting bistability of HS and LS configurations due to competition between the Pauli exclusion principle and the crystal field energy [66]. The external stimuli that induce such a phenomenon can be temperature, pressure, magnetic field, or emitting light [66–70]. Recently, ultrafast spin crossover has been observed in an unusual cationic cobalt-complex using femtosecond electronic and IR-vibrational (infrared) transient absorption spectroscopy [71], in which the very efficient coupling between the LS and HS states is attributed to the special situation that the Co_{II} complex is coordinated to a π-radical ligand. For the Co-Bz systems, which also exhibit strong $3d$-π interaction, such dynamics is promising to realize but in fact is quite challenging in our first-principle study. The difficulty lies in the fact that the transition between the initial and final states with different multiplicities (here singlets and triplets) is spin forbidden according to the selection rules. It only becomes allowed when low-lying d states with different multiplicities get mixed due to the inclusion of SOC.

After numerous trials and great efforts devoted to the four structures, we finally obtain a spin-crossover scenario in CoBz^+, as shown in Fig. 8(a). The whole process completes within around 600 fs with triplet state 12 and singlet state 76 as the initial and final state, respectively. The detailed information of the two states and the driving laser parameters for this dynamics can be found in Tables I and II, respectively. From the time-resolved occupation probabilities of the involved states [the upper panel of Fig. 8(a)], one can see that, after the influence of the laser pulses, the system ends at a linear combination of state 76 (i.e., the final state, with occupation 75%), state 11 (with occupation 19%), and the initial state (with probability 5%).

Inspecting the dynamic pattern we find there are mainly four couples of competing occupations (i.e., states 12 vs 11, states 11 vs 35, states 35 vs 13, and states 13 vs 76) during the whole scenario. Detailed analysis shows that the transfer pathway of the maximum population P_{max} of these states takes the form of a upward tilted W process, as depicted in Fig. 8(b), in which the involved states, their energies, spin multiplicities, and maximum transient occupations during the involution are indicated. Comparing with Fig. 8(a), we see that as soon as the laser is applied, state 11 dominates with a maximum occupation of 55% through a spin-flip-like dynamics via the Λ process (since a direct transition between state 12 and 11 is not or only weakly allowed due to the selection rule). Then, with the gradual involvement of other intermediate states, state 35 begins to prevail with a maximum occupation of 52% after

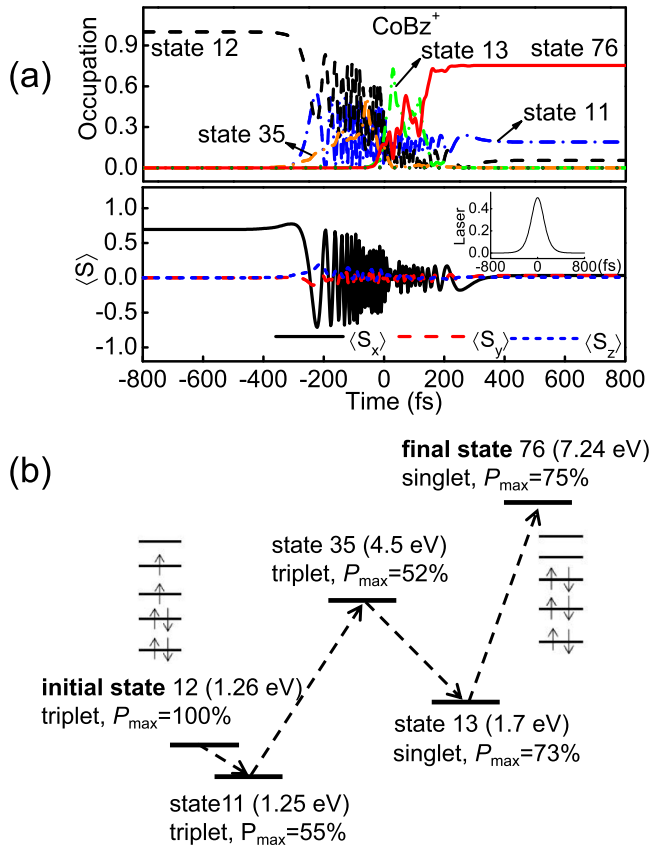

FIG. 8. (a) Spin-crossover scenario from triplet state (state 12, dashed black) to singlet state (state 76, red solid) in the structure $CoBz^+$. The mainly involved intermediate states with relatively high occupation during the propagation are indicated. (b) Schematic representation of the population transfer pathway of the main involved states during the whole dynamics process. The energies (in eV), multiplicities, and maximal transient occupation (P_{max}) of them are marked.

14 Rabi cycles between states 11 and 12. As stated previously in the analysis of the spin-switching dynamics in Fig. 4(a), one can find state 35 also contributes appreciably to the transition from state 12 to state 11, and this to some extent explains the appearance of many Rabi cycles between them. Here these three states are all triplet states before the inclusion of SOC. In the latter part of the dynamics, the singlet states come to take superior occupations. Specifically, competing with the occupation of state 35, the P_{max} of singlet state 13 gradually goes up and reaches a maximum value of 73%, and then an even higher occupation of the final state 76 with the final occupation 75% takes over via a two-photon Ξ process (since the energy difference of the last pathway is about twice of the laser energy). Such a multistepped W process facilitated dynamics, although complicated in behavior, induces a smaller laser detuning (thus a relatively low required laser energy 2.96 eV) than that of a normal Λ process. However, due to the difficulty to realize transitions between singlets and triplets, the intensity of the laser is relatively large (6.57 J s^{-1} m^{-2}). It should be emphasized that this W-type pathway of P_{max} of the involved states does not represent the time sequence of their participation during the whole spin-crossover scenario, and each path is not a simple direct transition between the states at its ends but a cooperative effect of all the involved, indispensable states.

In addition, depending on which way the six d electrons occupy the five nondegenerate orbitals caused by the C_{2v} symmetry of the system, the spin configuration can be either triplet or singlet [see Fig. 8(b)]. Here, with one electron missing in the cationic cluster, we consider six localized d electrons left for determining the spin state. The delocalized π electrons of Bz are usually paired and thus not relevant for spin. This is different from the charge density distribution as we discussed in Sec. III, for which the electron cloud is dispersed on both of the metal and ligand entities (Co: −0.249, Bz: −0.751), indicating an obvious separation of spin and charge.

The feasibility of this dynamics can be explained by the absorption spectra of the initial and final states [as shown in Fig. 7(b)]. From the spectra, one can clearly see there is no direct transition between states 12 and 76 since no peaks at energy positions of 5.599 eV for state 12 and −5.599 eV for state 76 are found, which reflects the spin-forbidden property of the singlet-triplet transition. However, their transition channel becomes open due to the involvement of the spin-mixed intermediate states. For example, four out of eight intermediate states, i.e., 34 (4.469 eV), 35 (4.498 eV), 36 (4.4983 eV), and 40 (4.582 eV), have both allowed transitions with states 12 and 76, which can be clearly seen from their common peaks around 4.5 eV (dashed frame) in Fig. 7(b).

V. SUMMARY

In summary, within the framework of a first-principles quantum chemistry method, we explore the structural, vibrational, energetic properties of cobalt-benzene clusters $CoBz^+$, $CoBz_2^+$, Co_2Bz, Co_2Bz_2, as well as their ultrafast laser-induced spin control. The four optimized structures are found to take the form of half-sandwich or sandwich geometries with multiplicity 3. The comparison and analysis of their conformations and vibrational spectra are performed, showing decent consistency with other theoretical and experimental work. Using the SACCI method, we calculate the structural-dependent ground and excited energy levels. They exhibit distinct distribution features as a result of different d-π interactions and electron configurations, which intrinsically leads to different spin dynamics with respect to the functional type, dynamic behavior and required laser parameters. To be specific, ultrafast spin-flip scenarios are realized in all four structures driven by different sets of laser pulses, while a spin-flip-transfer process and a novel spin-crossover process are only achieved in Co2Bz and $CoBz^+$, respectively. The latter two scenarios are remarkable: One is the fastest one found and also necessitates the lowest laser energy. The other follows a tilted-W path, which is the combination of two two-photon processes (Λ and Ξ) and two one-photon processes (direct transitions). All these processes can be essential for designing cooperative all-spin based functionality by proper arrangement. In addition, the optical spectra of the corresponding initial and final states are also discussed in order to understand the transferability of the two processes. All these theoretical predictions are expected to provide a deep insight into the ultrafast spin dynamics in metal-ligand (half-)

sandwich clusters, promote their experimental realization, and step towards future device applications.

ACKNOWLEDGMENTS

We acknowledge financial support from the National Natural Science Foundation of China (No. 11504223, No. 11572251, and No. 11872309), Natural Science Basic Research Plan in Shaanxi Province (No. 2017JM1033), the Fundamental Research Funds for the Central Universities (No. 3102017JC1003, No. 3102017JC11001, and No. GK2018-01009), and the German Research Foundation (Deutsche Forschungsgemeinschaft, DFG) through the Transregional Collaborative Research Center SFB/TRR 173 "Spin+X".

APPENDIX

As stated in Sec. IV A for the spin-flip scenario in the structure $CoBz^+$, the involvement of singlets does only slightly affect the dynamic behavior and the laser parameters (intensity, FWHM and energy). Here a flip scenario with an occupation probability of 98.9% is achieved in the triplet subspace, as shown in Fig. 9. The initial and final states are the same as in Fig. 4(a) since in the singlet-triplet subspace there are no singlet states below them. In this scenario, it is found that the number of the involved intermediate states is 3, and the parameters of the optimized laser pulse are: $\theta = 258.3°$, $\phi = 10.6°$, $\gamma = 165.4°$, Intensity $= 1.051$ J s^{-1} m^{-2}, FWHM $=$ 500 fs, $E_{\text{laser}} = 2.97$ eV. By comparing Figs. 4(a) and 9, one can clearly see, although ten singlets (along with additional six triplet states) are involved in the former scenario, their dynamic behavior, laser intensity, FWHM, and laser energy (see Table II) are almost the same. The only noticeable change is the laser orientation, however, when considering the C_{2v} symmetry of the structure, these two sets of laser angles are nearly equivalent. Thus it can be deduced that the spin-flip scenarios with the same initial and final states obtained in triplet subspace and singlet-triplet subspace usually exhibit the same feature. This is also the reason why we prefer to perform and discuss our dynamics in triplet subspace first and would extend to multiple subspace only when new types of spin scenarios are found there.

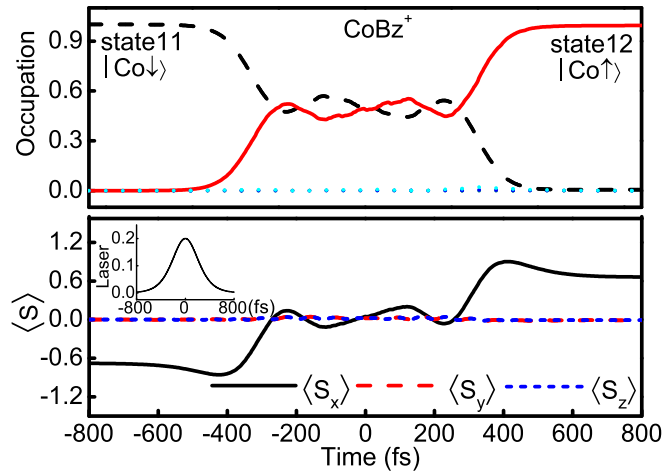

FIG. 9. Spin-flip process in clusters $CoBz^+$ within the triplet subspace.

[1] E. Beaurepaire, J.-C. Merle, A. Daunois, and J.-Y. Bigot, Phys. Rev. Lett. **76**, 4250 (1996).
[2] G. P. Zhang and W. Hübner, Phys. Rev. Lett. **85**, 3025 (2000).
[3] B. Koopmans, J. J. M. Ruigrok, F. Dalla Longa, and W. J. M. de Jonge, Phys. Rev. Lett. **95**, 267207 (2005).
[4] C. D. Stanciu, A. Tsukamoto, A. V. Kimel, F. Hansteen, A. Kirilyuk, A. Itoh, and T. Rasing, Phys. Rev. Lett. **99**, 217204 (2007).
[5] J.-Y. Bigot, M. Vomir, and E. Beaurepaire, Nat. Phys. **5**, 515 (2009).
[6] G. Lefkidis, G. P. Zhang, and W. Hübner, Phys. Rev. Lett. **103**, 217401 (2009).
[7] A. Kirilyuk, A. V. Kimel, and T. Rasing, Rev. Mod. Phys. **82**, 2731 (2010).
[8] U. Atxitia and O. Chubykalo-Fesenko, Phys. Rev. B **84**, 144414 (2011).
[9] T. Roth, A. J. Schellekens, S. Alebrand, O. Schmitt, D. Steil, B. Koopmans, M. Cinchetti, and M. Aeschlimann, Phys. Rev. X **2**, 021006 (2012).
[10] B. Pfau, S. Schaffert, L. Müller, C. Gutt, A. Al-Shemmary, F. Büttner, R. Delaunay, S. Düsterer, S. Flewett, R. Frömter *et al.*, Nat. Commun. **3**, 1100 (2012).
[11] A. Eschenlohr, M. Battiato, P. Maldonado, N. Pontius, T. Kachel, K. Holldack, R. Mitzner, A. Föhlisch, P. M. Oppeneer, and C. Stamm, Nat. Mater. **12**, 332 (2013).
[12] C.-H. Lambert, S. Mangin, B. S. D. C. S. Varaprasad, Y. K. Takahashi, M. Hehn, M. Cinchetti, G. Malinowski, K. Hono, Y. Fainman, M. Aeschlimann, and E. E. Fullerton, Science **345**, 1337 (2014).
[13] O. Morandi and P.-A. Hervieux, Phys. Rev. B **96**, 024441 (2017).
[14] W. Hübner, S. Kersten, and G. Lefkidis, Phys. Rev. B **79**, 184431 (2009).
[15] D. Chaudhuri, G. Lefkidis, and W. Hübner, Phys. Rev. B **96**, 184413 (2017).
[16] A. A. Khajetoorians, J. Wiebe, B. Chilian, and R. Wiesendanger, Science **332**, 1062 (2011).
[17] W.-H. Soe, C. Manzano, A. De Sarkar, F. Ample, N. Chandrasekhar, N. Renaud, P. de Mendoza, A. M. Echavarren, M. Hliwa, and C. Joachim, Phys. Rev. B **83**, 155443 (2011).
[18] G. D. Mahan, Phys. Rev. Lett. **102**, 016801 (2009).
[19] C. Li, S. B. Zhang, W. Jin, G. Lefkidis, and W. Hübner, Phys. Rev. B **89**, 184404 (2014).
[20] C. Joachim, Nanotechnology **13**, R1 (2002).
[21] T. Kurikawa, M. Hirano, H. Takeda, K. Yagi, K. Hoshino, A. Nakajima, and K. Kaya, J. Phys. Chem. **99**, 16248 (1995).
[22] T. Kurikawa, H. Takeda, M. Hirano, K. Judai, T. Arita, S. Nagao, A. Nakajima, and K. Kaya, Organometallics **18**, 1430 (1999).
[23] A. Nakajima and K. Kaya, J. Phys. Chem. A **104**, 176 (2000).

[24] M. Gerhards, O. C. Thomas, J. M. Nilles, W.-J. Zheng, and K. Bowen, J. Chem. Phys. **116**, 10247 (2002).

[25] T. D. Jaeger, D. van Heijnsbergen, S. J. Klippenstein, G. von Helden, G. Meijer, and M. A. Duncan, J. Am. Chem. Soc. **126**, 10981 (2004).

[26] S. T. Akin, V. Zamudio-Bayer, K. Duanmu, G. Leistner, K. Hirsch, C. Bülow, A. Ławicki, A. Terasaki, B. von Issendorff, D. G. Truhlar, J. T. Lau, and M. A. Duncan, J. Phys. Chem. Lett. **7**, 4568 (2016).

[27] R. Pandey, B. K. Rao, P. Jena, and M. A. Blanco, J. Am. Chem. Soc. **123**, 3799 (2001).

[28] J. Zhou, W.-N. Wang, and K.-N. Fan, Chem. Phys. Lett. **424**, 247 (2006).

[29] K. M. Wedderburn, S. Bililign, M. Levy, and R. J. Gdanitz, Chem. Phys. **326**, 600 (2006).

[30] X. Y. Zhang and J. L. Wang, J. Phys. Chem. A **112**, 296 (2008).

[31] R. J. Xiao, D. Fritsch, M. D. Kuz'min, K. Koepernik, H. Eschrig, M. Richter, K. Vietze, and G. Seifert, Phys. Rev. Lett. **103**, 187201 (2009).

[32] R. J. Xiao, D. Fritsch, M. D. Kuz'min, K. Koepernik, M. Richter, K. Vietze, and G. Seifert, Phys. Rev. B **82**, 205125 (2010).

[33] M. Karolak, D. Jacob, and A. I. Lichtenstein, Phys. Rev. Lett. **107**, 146604 (2011).

[34] I. S. Youn, D. Y. Kim, N. J. Singh, S. W. Park, J. Youn, and K. S. Kim, J. Chem. Theory Comput. **8**, 99 (2012).

[35] P. Shao, X.-Y. Kuang, and L.-P. Ding, J. Phys. Chem. A **117**, 12998 (2013).

[36] L. Horváthová, M. Dubecký, L. Mitas, and I. Štich, J. Chem. Theory Comput. **9**, 390 (2013).

[37] R. Flores and M. Castro, J. Mol. Struct. **1125**, 47 (2016).

[38] M. Karolak and D. Jacob, J. Phys: Condens. Matter **28**, 445301 (2016).

[39] J. W. González, T. Alonso-Lanza, F. Delgado, F. Aguilera-Granja, and A. Ayuela, Phys. Chem. Chem. Phys. **19**, 14854 (2017).

[40] A. N. Rudenko, F. J. Keil, M. I. Katsnelson, and A. I. Lichtenstein, Phys. Rev. B **86**, 075422 (2012).

[41] C. Li, J. Liu, S. B. Zhang, G. Lefkidis, and W. Hübner, Carbon **87**, 153 (2015).

[42] W. Jin, F. Rupp, K. Chevalier, M. M. N. Wolf, M. C. Rojas, G. Lefkidis, H.-J. Krüger, R. Diller, and W. Hübner, Phys. Rev. Lett. **109**, 267209 (2012).

[43] W. Jin, C. Li, G. Lefkidis, and W. Hübner, Phys. Rev. B **89**, 024419 (2014).

[44] A. K. Kandalam, B. Kiran, P. Jena, X. Li, A. Grubisic, and K. H. Bowen, J. Chem. Phys. **126**, 084306 (2007).

[45] H. Johll, H. C. Kang, and E. S. Tok, Phys. Rev. B **79**, 245416 (2009).

[46] H. C. Kandpal, K. Koepernik, and M. Richter, Phys. Rev. B **86**, 235430 (2012).

[47] T. Alonso-Lanza, Á. Mañanes, and A. Ayuela, J. Phys. Chem. C **121**, 18900 (2017).

[48] V. V. Maslyuk, A. Bagrets, V. Meded, A. Arnold, F. Evers, M. Brandbyge, T. Bredow, and I. Mertig, Phys. Rev. Lett. **97**, 097201 (2006).

[49] H. J. Xiang, J. L. Yang, J. G. Hou, and Q. S. Zhu, J. Am. Chem. Soc. **128**, 2310 (2006).

[50] G. Lefkidis and W. Hübner, Phys. Rev. B **76**, 014418 (2007).

[51] C. Li, W. Jin, H. P. Xiang, G. Lefkidis, and W. Hübner, Phys. Rev. B **84**, 054415 (2011).

[52] M. J. Frisch, G. W. Trucks, H. B. Schlegel, G. E. Scuseria, M. A. Robb, J. R. Cheeseman, G. Scalmani, V. Barone, G. A. Petersson, H. Nakatsuji, X. Li, M. Caricato, A. V. Marenich, J. Bloino, B. G. Janesko, R. Gomperts, B. Mennucci, H. P. Hratchian, J. V. Ortiz, A. F. Izmaylov, J. L. Sonnenberg, D. Williams-Young, F. Ding, F. Lipparini, F. Egidi, J. Goings, B. Peng, A. Petrone, T. Henderson, D. Ranasinghe, V. G. Zakrzewski, J. Gao, N. Rega, G. Zheng, W. Liang, M. Hada, M. Ehara, K. Toyota, R. Fukuda, J. Hasegawa, M. Ishida, T. Nakajima, Y. Honda, O. Kitao, H. Nakai, T. Vreven, K. Throssell, J. A. Montgomery, Jr., J. E. Peralta, F. Ogliaro, M. J. Bearpark, J. J. Heyd, E. N. Brothers, K. N. Kudin, V. N. Staroverov, T. A. Keith, R. Kobayashi, J. Normand, K. Raghavachari, A. P. Rendell, J. C. Burant, S. S. Iyengar, J. Tomasi, M. Cossi, J. M. Millam, M. Klene, C. Adamo, R. Cammi, J. W. Ochterski, R. L. Martin, K. Morokuma, O. Farkas, J. B. Foresman, and D. J. Fox, "Gaussian 16 Revision B.01", (2016), Gaussian Inc., Wallingford CT.

[53] H. Nakatsuji, Chem. Phys. Lett. **67**, 329 (1979).

[54] S. Koseki, M. W. Schmidt, and M. S. Gordon, J. Phys. Chem. A **102**, 10430 (1998).

[55] G. Lefkidis and W. Hübner, Phys. Rev. Lett. **95**, 077401 (2005).

[56] J. R. Cash and A. H. Karp, ACM Trans. Math. Software **16**, 201 (1990).

[57] T. Hartenstein, C. Li, G. Lefkidis, and W. Hübner, J. Phys. D: Appl. Phys. **41**, 164006 (2008).

[58] I. Valencia, Chem. Phys. **476**, 46 (2016).

[59] I. Valencia and M. Castro, J. Phys. Chem. A **114**, 13303 (2010).

[60] P. W. Anderson, Phys. Rev. **79**, 350 (1950).

[61] J. B. Goodenough, J. Phys. Chem. Sol. **6**, 287 (1958).

[62] J. Kanamori, J. Phys. Chem. Sol. **10**, 87 (1959).

[63] D. Dutta, M. Becherer, D. Bellaire, F. Dietrich, M. Gerhards, G. Lefkidis, and W. Hübner, Phys. Rev. B **97**, 224404 (2018).

[64] J. F. Létard, P. Guionneau, and L. Goux-Capes, Towards spin crossover applications, in *Spin Crossover in Transition Metal Compounds III*, Topics in Current Chemistry, Vol. 235 (Springer, Berlin, Heidelberg, 2004), pp. 221–249.

[65] A. Bousseksou, G. Molnár, L. Salmon, and W. Nicolazzi, Chem. Soc. Rev. **40**, 3313 (2011).

[66] J. L. Her, Y. H. Matsuda, M. Nakano, Y. Niwa, and Y. Inada, J. Appl. Phys. **111**, 053921 (2012).

[67] C. Sousa, C. de Graaf, A. Rudavskyi, R. Broer, J. Tatchen, M. Etinski, and C. M. Marian, Chem. Eur. J. **19**, 17541 (2013).

[68] T. Liu, H. Zheng, S. Kang, Y. Shiota, S. Hayami, M. Mito, O. Sato, K. Yoshizawa, S. Kanegawa, and C. Y. Duan, Nat. Commun. **4**, 2826 (2013).

[69] P. Gütlich, A. Gaspar, and Y. Garcia, Beilstein J. Org. Chem. **9**, 342 (2013).

[70] K. S. Kjær, W. K. Zhang, R. Alonso-Mori, U. Bergmann, M. Chollet, R. G. Hadt, R. W. Hartsock, T. Harlang, T. Kroll, K. Kubiček, H. T. Lemke, H. W. Liang, Y. Z. Liu, M. M. Nielsen, J. S. Robinson, E. I. Solomon, D. Sokaras, T. B. van Driel, T.-C. Weng, D. L. Zhu, P. Persson, K. Wärnmark, V. Sundström, and K. J. Gaffney, Struct. Dyn. **4**, 044030 (2017).

[71] F. Rupp, K. Chevalier, M. Graf, M. Schmitz, H. Kelm, A. Grün, M. Zimmer, M. Gerhards, C. van Wüllen, H.-J. Krüger, and R. Diller, Chem. Eur. J. **23**, 2119 (2017).